

Selective Modification of Halloysite Lumen with Octadecylphosphonic Acid: New Inorganic Tubular Micelle

Weng On Yah,[§] Atsushi Takahara,^{*,§,†,||} and Yuri M. Lvov^{*,‡}

[§]Graduate School of Engineering and [†]Institute of Materials Chemistry and Engineering, Kyushu University, 744 Motooka, Nishi-ku, Fukuoka 819-0395, Japan

^{||}International Institute for Carbon-Neutral Energy Research (WPI-I²CNER), Kyushu University, 744 Motooka, Nishi-ku, Fukuoka 819-0395, Japan

[‡]Institute for Micromanufacturing, Louisiana Tech University, 911 Hergot Avenue, Ruston, Louisiana 71272, United States

Supporting Information

ABSTRACT: Selective fatty acid hydrophobization of the inner surface of tubule halloysite clay is demonstrated. Aqueous phosphonic acid was found to bind to alumina sites at the tube lumen and did not bind the tube's outer siloxane surface. The bonding was characterized with solid-state nuclear magnetic resonance (²⁹Si, ¹³C, ³¹P NMR), Fourier transform infrared (FTIR), and X-ray photoelectron spectroscopy. NMR and FTIR spectroscopy of selectively modified tubes proved binding of octadecylphosphonic acid within the halloysite lumen through bidentate and tridentate P–O–Al linkage. Selective modification of the halloysite clay lumen creates an inorganic micelle-like architecture with a hydrophobic aliphatic chain core and a hydrophilic silicate shell. An enhanced capacity for adsorption of the modified halloysite toward hydrophobic derivatives of ferrocene was shown. This demonstrates that the different inner and outer surface chemistry of clay nanotubes can be used for selective modification, enabling different applications from water purification to drug immobilization and controlled release.



INTRODUCTION

Tubule halloysite clay has garnered interest in material science due to its versatile features of large surface area, high porosity, and tunable surface chemistry which enabled this nanomaterial to be utilized as a catalyst,¹ in electronic devices,² for entrapment of hydrophilic and lipophilic active agents,³ and as a nanofiller for polymers.⁴ Halloysite comprises naturally occurring aluminosilicate nanotubes with a 1:1 Al:Si ratio and a stoichiometry of $\text{Al}_2\text{Si}_2\text{O}_5(\text{OH})_4 \cdot n\text{H}_2\text{O}$. Halloysite occurs mainly in two polymorphs: the anhydrous form, with and interlayer of 7 Å, and the hydrated form, with expanded interlayer spacing of 10 Å, as a result of the incorporation of water in the interlamellar space.^{4d–f} Halloysite tubes consist of gibbsite octahedral sheet (Al–OH) groups on the internal surface and siloxane groups (Si–O–Si) on the external surface as shown in Figure 1.⁵ This difference results in a negatively charged outer surface and a positively charged inner lumen in the pH range 2–8. Interestingly, halloysite nanotubes have surface chemistry opposite to that of imogolite.⁶

Addition of 4–5% clay nanotubes into plastics typically doubles the composite strength and halloysite capacity to encase and release chemically active agents in a sustained manner, promising new functional nanocomposite materials. Recent studies have shown that halloysite is a biocompatible material; thus it is attractive for biotechnology, pharmaceutical, and medical research.⁷ The medical applications of these clay nanotubes include cancer cell separation, bone implants, cosmetics, and controlled drug delivery.⁸ Halloysite biocompo-

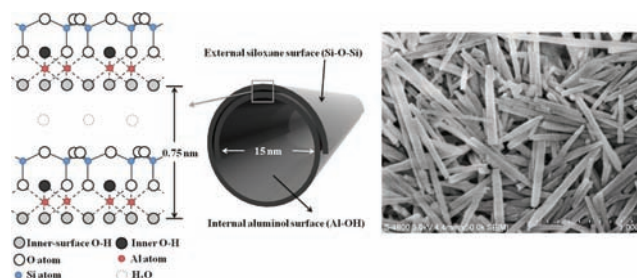


Figure 1. (Left) Schematic illustration of crystalline structure and (right) FE-SEM image of halloysite nanotubes.

sites⁹ are perspective materials with the great advantages that they are derived from natural resources, environmentally friendly, and available at low cost.¹⁰

Selective modification with functional molecules for different surfaces offers great promise for organic/inorganic composites (for example, simultaneous selective modification of gold–metal oxide systems based on high affinity of thiols for the gold surface and of carboxylic acid for the oxide areas).¹¹ Sequential bifunctionalization of Al–SiO₂/Si surfaces first by thiols and then by organosilanes and area-selective binding of organosilanes to oxidized areas of Si(111)-H surfaces have also been reported.¹² Recently, silane hydrophobization of single-wall

Received: November 12, 2011

Published: December 19, 2011

imogolite nanotube lumen was demonstrated.^{11c} A possibility to produce halloysite tubes with hydrophobized lumen will widen their applications as nanocontainers for nonpolar chemicals and for water purification.

Halloysite nanotubes having aluminum innermost and silicate outermost surfaces allow for different inner/outer surface chemistry. Selective modification between silica and alumina in halloysite is difficult. Attempts to use organosilanes for aluminosilicate surface modification resulted in silane binding to both inner and outer surfaces.¹³ Organophosphorus compounds are more promising for selective binding because they react selectively with TiO₂ areas of prepatterned TiO₂/SiO₂ substrates.¹⁴ Due to the high affinity of organophosphorus molecules toward metal oxide surfaces, aluminosilicate clays are expected to present similar selectivity. The use of organophosphonic acids in selective modification is attractive for preparation of highly hydrolytic stable hybrid materials, the lumen modification of which can be performed in water at ambient conditions, in contrast to organosilane coupling agents.

Inorganic micelle-like tubes with inner aliphatic chains and outer hydrophilic silicate shells were prepared through selective alkylphosphonic acid modification of the Al₂O₃ surface of halloysite inner lumen. The micellar features of modified halloysite are associated with its unique architecture, in which the hydrophobic lumen allows encapsulation of neutral and hydrophobic guest molecules by partitioning from a polar solvent, while the solid polar shell provides stability of the nanotube dispersion in water and retains the guest molecules. The stability of conventional organic micelles, which are characterized by a hydrophobic core and hydrophilic palisade architecture, depends on many parameters, such as solvent polarity, critical micelle concentration, and temperature. It is a rather fluid system; cross-linking may increase micelle stability, but it may also cause safety concerns because many cross-linkers are toxic. Our tubule clay micelle-like absorbent offers additional features, such as chemical and mechanical stability and the possibility to produce this material in large quantities. To characterize specific adsorption and release properties of clay nanotubes with a hydrophobized interior, we used hydrophobic and hydrophilic ferrocene derivatives which were loaded into the halloysite.

Previously, ferrocene derivatives have been included in long-chain alkanes to study the electron-transfer reactions of redox species in a nonpolar environment.¹⁵ Ferrocenyl and multi-ferrocenyl systems have been used as redox sensors for molecular recognition, as building blocks in polymers, and as electron donors for push–pull nonlinear optical chromophores. Ferrocene shows biological activity and has been used in hematinic, antimicrobial, antitumor, and anticancer agents for potential cancer treatments.¹⁶

To develop selective surface modification of clay nanotubes, we demonstrated grafting different organic groups to mixed oxide surfaces of halloysite through successive reactions with phosphonic acid (interior) and silylating (exterior) agents. Such a selective bifunctionalization of halloysite nanotubes allows production of a new type of adsorbent with tunable properties.

EXPERIMENTAL SECTION

Materials. Processed halloysite was provided by Applied Minerals Inc., USA, and used without further treatment. Octadecylphosphonic acid (ODP), ferrocene (FC), and ferrocenecarboxylic acid (FCA) were purchased from Aldrich Chemicals and used without further purification. Tetrahydrofuran (THF) and ethanol were also obtained

from Aldrich Chemicals. *N*-(2-Aminoethyl)-3-aminopropyltrimethoxysilane (AEAPS) was obtained from Shin-Etsu Chemical Co. Ltd. and used as received.

Modification of Halloysite Lumen with Octadecylphosphonic Acid. Halloysite (500 mg) was added under stirring to a solution of the octadecylphosphonic acid (2 mmol) in 500 mL of 4:1 EtOH:H₂O. The EtOH:H₂O solution was adjusted to pH 4. The halloysite suspension was transferred to a vacuum jar, which was then evacuated using a vacuum pump. The fizzing of the suspension indicated that air has been removed from the lumen of the halloysite tubules and replaced with ODP solution.³ The process of air evacuation and cycling back to atmospheric pressure was repeated three times in order to maximize ODP in the halloysite lumen. After stirring for a week at room temperature, the modified halloysite was rinsed, centrifuged five times with EtOH:H₂O, and dried at 100 °C overnight under vacuum. The final product was denoted as halloysite-ODP. Halloysite-ODP aqueous suspension showed colloidal stability similar to that of untreated halloysite, indicating that the outermost surface of the clay nanotube was not hydrophobized.

Grafting of Organosilane to External Surface of Halloysite-ODP. Further modification of halloysite-ODP by AEAPS was performed according to a previously reported procedure.^{17b} First, 0.3 mL of AEAPS dissolved in 80 mL of dry toluene was combined with 1 g of dried halloysite-ODP in a glovebox. The suspension was dispersed ultrasonically for 20 min at room temperature and heated at 75 °C under constant stirring for 20 h. The powder was filtered, rinsed with 300 mL of toluene to remove excess AEAPS, and then dried at 100 °C under vacuum.

RESULTS AND DISCUSSION

Structural and Morphological Characterization. Transmission electron microscopy (TEM) images reveal that halloysite is a cylindrical-shaped tube with multilayer walls and an open-ended lumen along the nanotube. The samples contain agglomerates of nanotubes with some irregularity in diameter, wall thickness, and morphology. The tubes have an external diameter of 40–60 nm and an inner diameter of 15–20 nm, while the wall thickness is about 20 nm. Overall, the morphology parameters of our halloysite sample are identical to those of previously reported samples.^{1,3} After modification of halloysite, the transparent central channel (Figure 2a) that runs

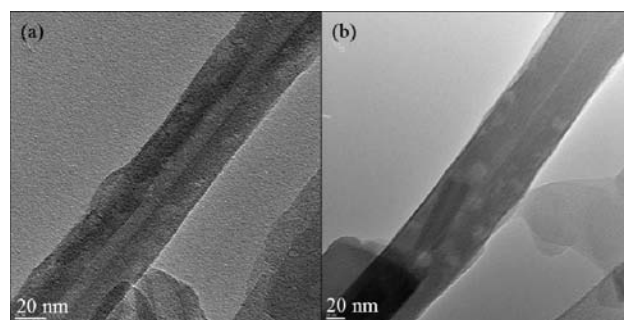


Figure 2. TEM images of (a) original halloysite and (b) halloysite-ODP.

longitudinally along the nanotube becomes less resolved (Figure 2b), indicating that the lumen has been covered with a less dense layer, like an organic material. Later, with spectroscopic data, we will prove that the layer is bound ODP. Judging from the TEM images, the lumen is not completely filled or blocked, which may be beneficial for loading/release applications.

The porosity of halloysite before and after ODP modification was measured by N₂ adsorption–desorption at 77 K (Figure

S1, Supporting Information). The isotherm of halloysite and halloysite-ODP is of type II with H3 hysteresis loops, according to IUPAC classification.¹⁷ The BET specific surface area (S_{BET}) and pore volume (V_{pore}) of untreated halloysite are 43 cm²/g and 0.53 cm³/g, respectively. The isotherm of halloysite-ODP is similar to that of original halloysite, with lower S_{BET} and V_{pore} of 27.6 cm²/g and 0.38 cm³/g, respectively. The pore distribution curve shows one primary population of pores at 32 ± 1 and 28 ± 1 nm for halloysite and halloysite-ODP, respectively (Table S1, Supporting Information). A 4 nm reduction in pore diameter of halloysite after modification indicates the formation of a single grafted ODP layer.¹⁸ Although the values calculated by N₂ adsorption are biased toward maximum diameter compared to values observed by TEM images, it is clear that these values have more statistical significance for larger size samples.

X-ray Diffraction. Original halloysite exhibits (001) diffraction peak at $q = 8.33 \text{ nm}^{-1}$, corresponding to a multilayer wall spacing of 0.72 nm, which identifies it as halloysite-7 Å¹⁹ (Figure S2, Supporting Information). The diffraction patterns in Figure S2 show that the spacing of modified halloysite-ODP remained unchanged, indicating that no intercalation of ODP into the interlayer of tube walls occurs. This suggests that most of the wall interlayer AlOH groups of halloysite are unavailable for grafting.

Spectroscopic Data on ODP Immobilization. *X-ray Photoelectron Spectroscopy (XPS).* The wall thickness is estimated as 20 nm, which well exceeds the penetration depth of XPS (10 nm). Thus, it is difficult to disclose the chemical composition of the inner lumen surface where the bonding of ODP occurs. Nevertheless, since halloysite is oriented randomly on a substrate, the inner surface may be partially exposed to X-rays. Each silicon atom in halloysite is coordinated to four oxygen atoms, and each aluminum atom is coordinated to two hydroxyl groups and one oxygen atom (Figure 1).²⁰ Surface chemical compositions of the samples were determined (Table 1). Oxygen, silicon, and aluminum are

Table 1. Atomic Percent Concentration (%) for Elements O 1s, C 1s, P 2p, Si 2p, and Al 2p of Halloysite and Halloysite-ODP

	O	Si	Al	C	P
original halloysite	67.0	16.5	9.3	7.2	<0.1
halloysite-ODP	34.6	28.7	1.3	34.1	1.7

the main elements detected, with a Si/Al ratio of about 1.75, higher than unity, indicating the presence of a surface rich in silicon. The results show that original halloysite had a small amount of carbon (Figure 3a), and that carbon contamination likely occurred during sample preparation in the presence of air.

After adsorption of ODP (Figure 3b), the intensity of C 1s at a binding energy of 286.8 eV increased significantly, with detection of a weak P 2p peak at a binding energy of 137 eV, a key indication of the presence of phosphonate on halloysite. Compared with the theoretical value calculated from the stoichiometry of C₁₈H₃₉O₃P molecules, the C/P elemental ratio provides a check on the chemical composition of the grafted layer. The elemental ratio of C/P for halloysite-ODP is 20, approaching the theoretical value of 18 with the deviation attributed to the hydrocarbon contamination. The main Si 2p peak at 107 eV is attributed to Si–O–Si/Si–O–Al.²¹ The Si 2p of halloysite-ODP is similar to that of the original nontreated

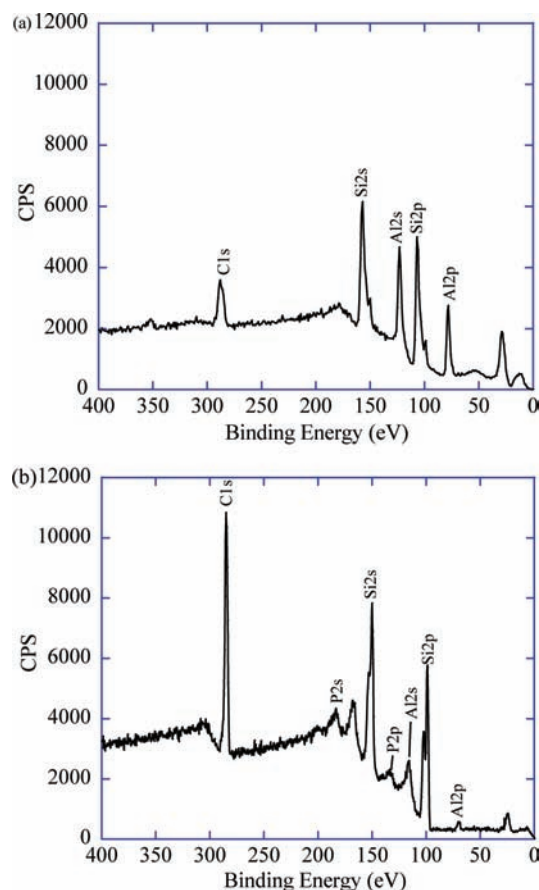


Figure 3. XPS spectra taken for (a) unmodified halloysite and (b) halloysite-ODP.

halloysite. No additional component can be assigned to a Si–O–P bond at a binding energy of 103 eV, as reported in the literature.²² It can be concluded that no Si–O–P formation occurred on the outer surface of halloysite.

FTIR Spectroscopy. Figure 4a shows the methylene stretching region of ODP and halloysite-ODP. The methylene groups are known to give two bands corresponding to symmetric and asymmetric C–H stretching at 2850–2852 and 2916–2924 cm^{−1}, respectively. In the same region, terminal methyl groups of symmetric and asymmetric stretching modes are detected at 2872 and 2958 cm^{−1}. All three frequencies of ODP are shifted toward lower values, which indicates a more constricted vibration of alkyl groups inside the confined spaces of halloysite lumen (Supporting Information, Figure S4, Table S3; the frequency and assignment of each vibrational mode observed are also listed in the Supporting Information).²³

The dramatic decreases of the P–O–H peak at 2375–2200 cm^{−1} and the P=O vibration at 1228 cm^{−1} could indicate that the binding mode is mostly tridentate (Figure 4b). Definite assignments of these bands are difficult since the ranges for the different P–O stretching peaks overlap and depend on the degree of hydrogen bonding.

¹³C Solid-State NMR. A difference in the degree of chain order of ODP adsorbed on halloysite internal surface is revealed by the ¹³C CPMAS NMR spectra, shown in Figure 5a. The domain of the ordered and disordered chains is resolved in the ¹³C CPMAS NMR spectra because the relative populations of trans and gauche conformations influence the ¹³C chemical shift of the interior methylene carbon. For ODP in the

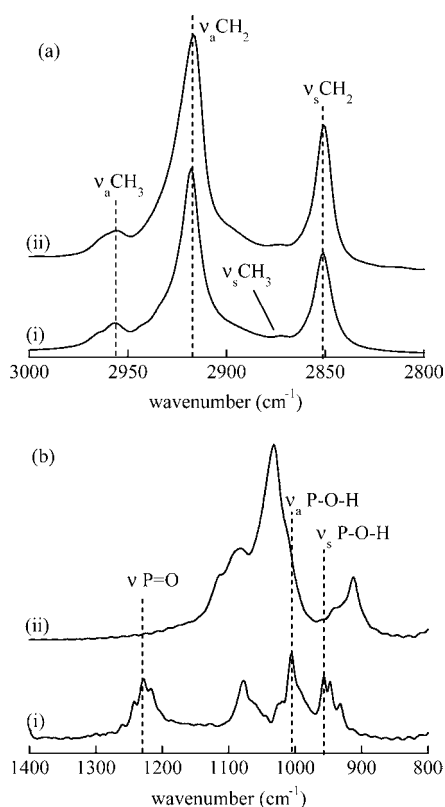


Figure 4. (a) Methylene stretching region (3000 to 2800 cm^{-1}) and (b) P–O stretching region (1400 to 800 cm^{-1}) of the FTIR of (i) ODP and (ii) halloysite-ODP.

crystalline state, these carbons resonate at 33–36 ppm for an all-trans conformation.²⁴ An intense peak at 35.2 ppm, corresponding to all-trans chains, is observed for ODP adsorbed in the lumen. Whereas a single methyl carbon peak at 16.8 ppm is present in the ^{13}C CPMAS NMR spectra of pure crystalline ODP, two methyl carbon peaks are observed at 14.3 and 16.5 ppm for halloysite-ODP. The upfield shift of the methyl group suggests conformational disorder at the chain terminals as compared to the methyls in ODP solid.²⁵

^{31}P Solid-State NMR. The ^{31}P solid-state NMR spectrum, shown in Figure 5b, reveals the nature of the interaction between the phosphonic acid headgroup and a metal oxide surface. ^{31}P chemical shifts are sensitive to variations in the O–P–O bond angle as well as to the electronegativity of the nearest atoms. ODP headgroups may act as mono-, bi-, or tridentate ligands on the alumina surface. Significant changes are observed for halloysite-ODP, where the phosphorus resonance is shifted further upfield and is inhomogeneously broadened. The peaks are shifted from those of the pure ODP, and an isotropic chemical shift at 33.0 ppm indicates a strong interaction with the alumina surface of halloysite lumen. The broad distribution of chemical shifts is due to different types of surface bonds and bonding sites on the alumina surface.²⁶ Based on the average upfield shifts of 6.2 and 10.3 ppm from free acid, the primary modes of ODP attachment to the alumina surface are bi- and tridentate. Similar ^{31}P resonance shifts have been observed in numerous studies where phosphonic acids were reacted with titania, alumina, SnO_2 , and zirconia surfaces.²⁷

^{29}Si MAS NMR. The ^{29}Si MAS NMR spectrum of the halloysite-ODP (Figure S5, Supporting Information) shows

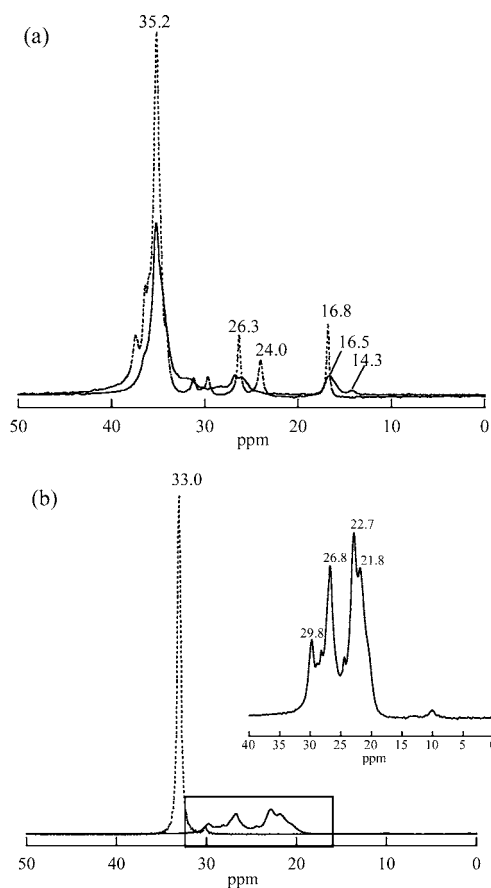


Figure 5. (a) ^{13}C CPMAS and (b) ^{31}P CPMAS NMR spectra of ODP (dotted line) and halloysite-ODP (solid line).

that there are no high-field resonances arising from higher coordinated Si atoms between -120 and -220 ppm. It rules out the possibility of phosphoryl groups binding to the silica surface, because the presence of phosphonate surface species bonded to silica, forming hexa-coordinated Si atoms, would give a chemical shift at -212 ppm.²⁸

Therefore, the following spectroscopic data indicate the formation of binding between phosphonic acid and the alumina internal surface of halloysite tubes: (1) the absence of a Si–O–P bond at the external surface of halloysite from XPS data, (2) a significant decrease of P–O–H and P=O vibrations, and (3) broadening and upfield shifting in the ^{31}P CP MAS NMR spectrum for halloysite-ODP.

Adsorption of Ferrocene Derivatives by Halloysite. To compare the adsorption of hydrophobic and hydrophilic ferrocene derivatives by original halloysite and halloysite-ODP, 1 mM solutions of ferrocene or ferrocenecarboxylic acid were added to 5, 10, 15, or 20 mg/mL halloysite samples. After 2 h of incubation, the samples were centrifuged. The intensities of the bands for ferrocene (235–250 nm) and ferrocenecarboxylic acid (305–320 nm) were obtained for each sample. The intensities of the halloysite were subtracted to give the absorption of the ferrocene remaining in solution (Figure 6). Assuming that ferrocene adsorption is proportional to the amount in halloysite samples, linear fits are shown for each sample (Table S5, Supporting Information).

The adsorption of ferrocene derivatives is affected by the polarity differences of the adsorbent and adsorbate. Ferrocene is more hydrophobic, and its adsorption was enhanced by

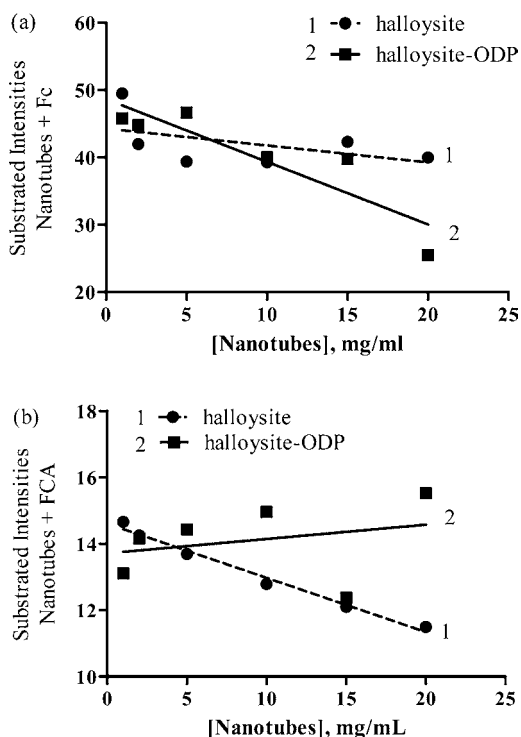


Figure 6. Band intensities of absorption of (a) ferrocene and (b) ferrocenecarboxylic acid remaining in solution after halloysite solids were centrifuged out. Various amounts of the halloysites (1, 2, 5, 10, 15, and 20 mg/mL) were added to 1 mM ferrocene/ferrocenecarboxylic acid.

hydrophobized lumen halloysite-ODP as compared with untreated halloysite. The halloysite-ODP has higher adsorption capacity for hydrophobic molecules because the hydrophobic tubular core acts like a sponge to embed ferrocene into its alkyl chains. Apparently, modified halloysite-ODP leads to faster adsorption of ferrocene compared to unmodified halloysite (Figure S8, Table S6, Supporting Information).

For a comparative study, the same experiment and calculations were performed for adsorption of ferrocenecarboxylic acid. This ferrocene derivative has polar moieties and is more hydrophilic than ferrocene. We found that untreated halloysite adsorbed more ferrocenecarboxylic acid than halloysite-ODP because of the favorable hydrogen bonding in the alumina lumen. The ODP-modified halloysite showed barely any adsorption compared to the parent unmodified halloysite (Figure 6b). The equilibrium adsorption of ferrocene by halloysite and halloysite-ODP is shown in Figure 7. The adsorption isotherms for both samples are linear, with correlation coefficients of 0.88 and 0.95 for halloysite and halloysite-ODP. The linearity of the adsorption isotherms is consistent with the idea that inclusion of ferrocene by the halloysite sample is a partitioning process, in which the hydrophobic ferrocenes distribute between the organic phase and aqueous phase. The dominant driving forces for the ferrocene adsorption are hydrophobic interaction and capillary forces, where hydrophobic guests are driven into the less polar lumen of halloysite-ODP. The slope difference between the isotherms shows that the partitioning equilibria favor the less polar environment of halloysite-ODP for hydrophobic ferrocene.

Raman Spectroscopy. Figure 8 depicts the low-frequency Raman spectra of ferrocene and ferrocene-halloysite-ODP

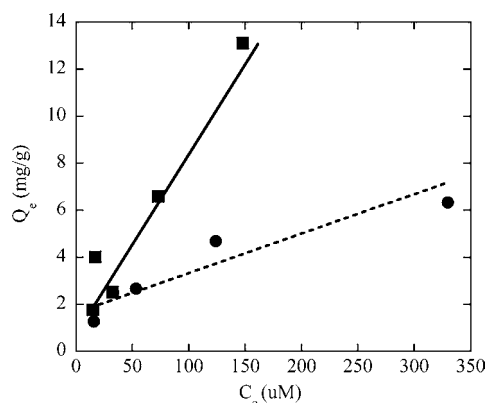


Figure 7. Equilibrium adsorption of ferrocene by halloysite (●) and halloysite-ODP (■) at room temperature from THF:H₂O (1:1) solution.

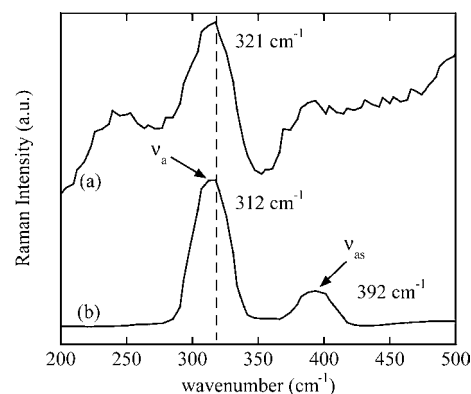


Figure 8. Low-frequency Raman spectra of (a) ferrocene-halloysite-ODP and (b) ferrocene. The ferrocene spectrum is downscaled for better visibility.

hybrid. The Raman spectrum of ferrocene within the modified halloysite-ODP is similar to that reported for ferrocene in the solution or solid state.²⁹ The low-frequency Raman spectrum of ferrocene solid shows two bands at 312 and 392 cm⁻¹, which correspond to the Fe–Cp stretching and Fe–Cp ring tilt, respectively.^{15a} For ferrocene-halloysite-ODP, the Raman signal is weaker than for the ferrocene powder because of shielding from the tube wall. We analyzed the strongest peak, at 312 cm⁻¹, in the low-frequency spectral region to confirm the ferrocene inclusion. The Fe–Cp stretch of ferrocene-halloysite-ODP at 321 cm⁻¹ is red-shifted in comparison to its position in ferrocene solid, signifying the elongation of the Fe–Cp distance for the ferrocene molecule when embedded into the alkyl chains of halloysite-ODP lumen. The band is also broadened, which indicates that interactions are present between ferrocene and alkyl chains.

Release of Ferrocene from Halloysite. Figure 9a shows the mass of ferrocene released from samples saturated with 20 mM ferrocene solution at room temperature. For original halloysite, only a small initial burst release is observed due to dissolution of the ferrocene from the halloysite surface. ODP-modified halloysite releases 4 times more ferrocene in the same period of time, indicating its higher adsorption capacity.

The release profiles of ferrocene correspond to diffusional release and were fitted with a non-Fickian transport model represented by the Higuchi equation.³⁰ This model suggests a dependence of guest release on the square root of time: $Q_t =$

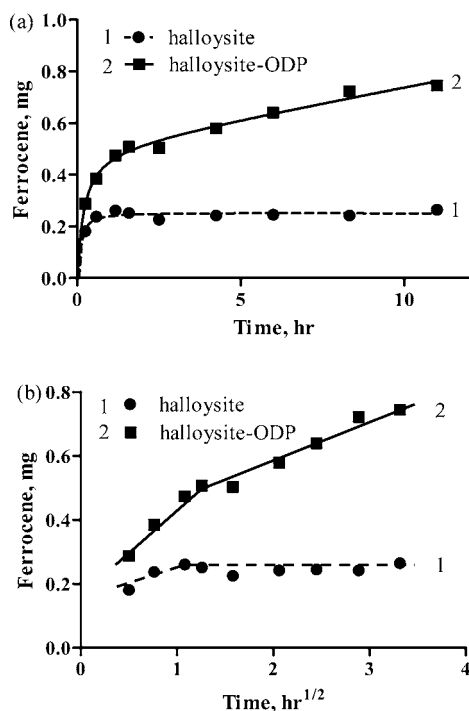


Figure 9. (a) Release profile and (b) Higuchi square root of time plots for release of ferrocene from halloysite (●) and halloysite-ODP (■).

$k_H t^{1/2}$, where k_H is the release rate. This equation has been applied for drug release from porous silica systems.³¹ A straight line in the plot corresponds to pure Higuchi type of diffusion-driven release where no alteration of the matrix occurs.

The Higuchi plot for halloysite-ODP displays a two-step release (Figure 9b), probably reflecting desorption of the outside surface and from the tube lumen. For original halloysite, the first linear region is followed by a horizontal line, indicating no release at the second stage. The ferrocene release rate is higher for the halloysite-ODP system than for the original halloysite. Data for unmodified halloysite did not fit well to the Higuchi equation, and its release behavior does not obey the diffusional release model (Table S7, Supporting Information). It is probable that the majority of the ferrocene was simply adsorbed on halloysite's external surface.

Bifunctionalization of Halloysite. After halloysite lumen modification through specific reaction of phosphonic acid with the alumina innermost surface, we made a consecutive treatment of the outermost silica surface through silanization. Reaction of halloysite-ODP with AEAPS resulted in the grafting of silyl groups, as evidenced by the signal at -64.6 ppm characteristic of hydrolyzed AEAPS (Figure S9, Supporting Information). Modification of the silica-rich external surface of halloysite with silyl groups demonstrates the possibility of bifunctionalization of halloysite, as illustrated in Figure 10.

CONCLUSIONS

Selective modification of an aluminosilicate clay nanotube's inner lumen with octadecylphosphonic acid was demonstrated. In this way we exploited different innermost/outermost surface chemistry of clay nanotubes. No octadecylphosphonic acid bonding was observed on the siloxane outer tube surface, as evidenced by solid-state NMR and XPS. Strong bidentate and tridentate Al–O–P bonds were detected on the alumina lumen surface of halloysite, since the weakly bound monodentate

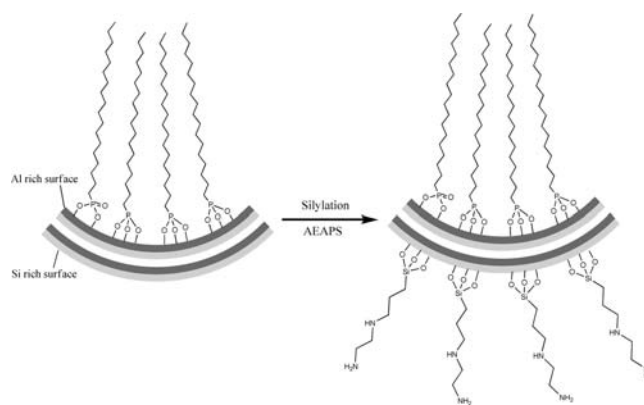


Figure 10. Schematic illustration of bifunctionalization of the silica–alumina oxide surface of halloysite by ODP and subsequent AEAPS silylation.

compounds were removed by sonication and rinsing. The adsorption study showed that halloysite with hydrophobic-modified lumen adsorbs more ferrocene than its hydrophilic derivative (ferrocenecarboxylic acid). Therefore, like in organic micelles, the octadecylphosphonic acid immobilized in the halloysite lumen may behave as a sponge for physisorption, increasing the adsorption capacity for hydrophobic molecules. The equilibrium uptake isotherm for ferrocene is linear, indicating that these molecules are driven into the lumen by partitioning from polar solvent. The release studies also showed that halloysite-ODP has higher ferrocene loading. Sequential treatment of halloysite with organosilane coupling agents offers a simple way to bind covalently a second class of organic groups on the silica outermost surface of these clay nanotubes.

ASSOCIATED CONTENT

Supporting Information

Experimental details; figures and tables showing N₂ adsorption–desorption isotherm, pore size distribution, wide-angle X-ray diffraction pattern, FTIR, ²⁹Si MAS NMR, UV–visible spectra of halloysite before and after modification, adsorption results of ferrocene and ferrocenecarboxylic acid, time dependence of adsorption, release rate of ferrocene by Higuchi equation, and ²⁹Si MAS NMR and ³¹P CPMAS NMR after consecutive silanization. This material is available free of charge via the Internet at <http://pubs.acs.org>.

AUTHOR INFORMATION

Corresponding Author

takahara@cstf.kyushu-u.ac.jp; ylvov@latech.edu

ACKNOWLEDGMENTS

The authors acknowledge the financial support of a Grant-in-Aid for Scientific Research (A) (No. 19205031) from Japan Society for the Promotion of Science. The present work is also supported by a Grant-in-Aid for GCOE Program, “Science for Future Molecular Systems”, from Ministry of Education, Culture, Science, Sports and Technology of Japan. Partial support by U.S. NSF-1029147 and EPS1003897 grants are acknowledged. The synchrotron radiation experiments were performed at SPring-8 (No. 2010A1454). The authors thank Dr. Elshad Abdullayev (LaTech) and Ms. Keiko Ideta of Evaluation Center of Materials Properties and Function,

Kyushu University, for their assistance in the work and Applied Minerals, Inc. for supplying halloysite.

REFERENCES

- (1) (a) Barrientos-Ramírez, S.; Ramos-Fernández, E. V.; Silvestre-Albero, J.; Sepúlveda-Escribano, A.; Pastor-Blas, M. M.; González-Montiel, A. *Microporous Mesoporous Mater.* **2009**, *120*, 132–140. (b) Machado, G. S.; Castro, K.; Wypych, F.; Nagasaki, S. *J. Mol. Catal. A: Chem.* **2008**, *283*, 99–107. (c) Shchukin, D. G.; Sukhorukov, G. B.; Price, R. R.; Lvov, Y. M. *Small* **2005**, *1*, 510–513. (d) Abdullayev, E.; Sakakibara, K.; Okamoto, K.; Wey, W.; Ariga, K.; Lvov, Y. *ACS Appl. Mater. Interfaces* **2011**, *3*, 4040–4046.
- (2) Wan, C.; Li, M.; Bai, X.; Zhang, Y. *J. Phys. Chem. C* **2009**, *113*, 16238–16246.
- (3) (a) Shamsi, M. H.; Geckeler, K. E. *Nanotechnology* **2008**, *19*, 075604–075608. (b) Veerabadrán, N. G.; Mongayt, D.; Torchilin, V.; Price, R. R.; Lvov, Y. *Macromol. Rapid Commun.* **2009**, *30*, 99–103. (c) Abdullayev, E.; Price, R.; Shchukin, S.; Lvov, Y. *ACS Appl. Mater. Interfaces* **2009**, *1*, 1437–1443. (d) Lvov, Y.; Shchukin, D.; Möhwald, H.; Price, R. *ACS Nano* **2008**, *2*, 814–820.
- (4) (a) Cavallaro, G.; Lazzara, G.; Milioto, S. *Langmuir* **2011**, *27*, 1158–1167. (b) Du, M.; Guo, B.; Jia, D. *Polym. Int.* **2010**, *59*, 574–582. (c) Wei, W.; Abdullayev, E.; Hollister, A.; Mills, D.; Lvov, Y. *Macromol. Mater. Eng.* **2012**, *302*, 342–353. (d) Churchman, G. J.; Carr, R. M. *Clays Clay Miner.* **1975**, *23*, 382–388. (e) Alexander, L. T.; Faust, G. T.; Hendrick, S. B.; Insley, H.; McMurdie, H. F. *Am. Mineral.* **1943**, *28*, 1–18. (f) Joussein, E.; Petit, S.; Churchman, J.; Theng, B.; Righi, D.; Delvaux, B. *Clay Miner.* **2005**, *40*, 383–426. (g) Cavallaro, G.; Donato, D.; Lazzara, G.; Milioto, S. *J. Phys. Chem. C* **2011**, *115*, 20491–20498.
- (5) (a) Hendricks, S. B. *Am. Mineral.* **1938**, *23*, 295–301. (b) Bates, T. F.; Hildebrand, F. A.; Swineford, A. *Am. Mineral.* **1950**, *35*, 463–484.
- (6) (a) Wada, K. *Am. Mineral.* **1969**, *54*, 50–71. (b) Cradwick, P. D. *G. Nature* **1972**, *240*, 187–189. (c) Yamamoto, K.; Otsuka, H.; Wada, S.; Takahara, A. *Chem. Lett.* **2001**, *30*, 1162–1163.
- (7) (a) Vergaro, V.; Abdullayev, E.; Lvov, Y. M.; Zeitoun, A.; Cingolani, R.; Rinaldi, R.; Leporatti, S. *Biomacromolecules* **2010**, *11*, 820–826. (b) Price, R. R.; Gaber, B. P.; Lvov, Y. M. *J. Microencapsulation* **2001**, *18*, 713–722. (c) Veerabadrán, N.; Price, R.; Lvov, Y. *Nano* **2007**, *2*, 215–222.
- (8) (a) Hughes, A. D.; King, M. R. *Langmuir* **2010**, *26*, 12155–12164. (b) Levis, S. R.; Deasy, P. B. *Int. J. Pharm.* **2002**, *243*, 125–134.
- (9) (a) Levis, R.; Deasy, P. B. *Int. J. Pharm.* **2003**, *253*, 145–157. (b) Kelly, H. M.; Deasy, P. B.; Ziaka, E.; Claffey, N. *Int. J. Pharm.* **2004**, *274*, 167–183.
- (10) Hassan-Nejad, M.; Ganster, J.; Bohn, A.; Pinnow, M.; Volkert, B. *Macromol. Symp.* **2009**, *280*, 123–129.
- (11) (a) Laibinis, P. E.; Hickman, J. J.; Wrighton, M. S.; Whitesides, G. M. *Science* **1989**, *245*, 845–847. (b) Gardner, T. J.; Frisbie, C. D.; Wrighton, M. S. *J. Am. Chem. Soc.* **1995**, *117*, 6927–6933. (c) Kang, D.-Y.; Zang, J.; Jones, C. W.; Nair, S. *J. Phys. Chem. C* **2011**, *115*, 7676–7685.
- (12) (a) Xia, Y.; Whitesides, G. M. *Adv. Mater.* **1996**, *8*, 765–768. (b) Ho, P. K. H.; Filas, R. W.; Abusch-Magder, D.; Bao, Z. *Langmuir* **2002**, *18*, 9625–9628. (c) Sugimura, H.; Nakagiri, N.; Ichinose, N. *Appl. Phys. Lett.* **1995**, *66*, 3686–3688. (d) Inoue, A.; Ishida, T.; Choi, N.; Mizutani, W.; Tokumoto, H. *Appl. Phys. Lett.* **1998**, *73*, 1976–1978.
- (13) (a) Johnson, L. M.; Pinnavaia, T. J. *Langmuir* **1990**, *6*, 307–311. (b) Johnson, L. M.; Pinnavaia, T. J. *Langmuir* **1991**, *7*, 2636–2641.
- (14) (a) Michel, R.; Lussi, J. W.; Csucs, G.; Reviakine, I.; Danuser, G.; Ketterer, B.; Hubbell, J. A.; Textor, M.; Spencer, N. D. *Langmuir* **2002**, *18*, 3281–3287. (b) Michel, R.; Reviakine, I.; Sutherland, D.; Fokas, C.; Csucs, G.; Danuser, G.; Spencer, N. D.; Textor, M. *Langmuir* **2002**, *18*, 8580–8586.
- (15) (a) Mohanambe, L.; Vasudevan, S. *Inorg. Chem.* **2005**, *44*, 2128–2130. (b) Podkoscielny, D.; Hooley, R. J.; Rebek, J. Jr.; Kaifer, A. E. *Org. Lett.* **2008**, *10*, 2865–2868.
- (16) (a) Weber, B.; Serafin, A.; Michie, J.; Rensburg, C. V.; Swarts, J. C.; Bohm, L. *Anticancer Res.* **2004**, *24*, 763–770. (b) Davis, W.; Shago, R. F.; Langer, E. H. G.; Swarts, J. C. *Polyhedron* **2005**, *24*, 1611–1616. (c) Wei, H.; Quan, C. -Y.; Chang, C.; Zhang, X. -Z.; Zhuo, R. -X. *J. Phys. Chem. B* **2010**, *114*, 5309–5314.
- (17) (a) Gregg, S. J.; Sing, K. S. W. *Adsorption, Surface Area and Porosity*, 2nd ed: Academic Press: London, 1982. (b) Yuan, P.; Southon, P. D.; Liu, Z.; Green, M. E. R.; Hook, J. M.; Antill, S. J.; Kepert, C. J. *J. Phys. Chem. C* **2008**, *112*, 15742–15751.
- (18) Ulman, A. *An Introduction to Ultrathin Organic Films: From Langmuir-Blodgett to Self Assembly*; Academic Press: San Diego, CA, 1991.
- (19) Brindley, G. W. Order-disorder in the clay mineral structures. In *Crystal Structures of Clay Minerals and Their X-ray Identification*; Brindley, G. W., Brown, G., Eds.; Mineralogist Society: London, 1980; p 125.
- (20) (a) Bates, T. F.; Hildebrand, F. A.; Swineford, A. *Am. Mineral.* **1950**, *35*, 463–484. (b) Singh, B. *Clays Clay Miner.* **1996**, *44*, 191–196. (c) Singh, B.; Gilkes, R. J. *Clays Clay Miner.* **1992**, *40*, 212–229. (d) Singh, B.; Mackinnon, I. D. R. *Clays Clay Miner.* **1996**, *44*, 825–834.
- (21) Wittberg, T. N.; Wang, P. S. *Surf. Interface Anal.* **1999**, *27*, 936–940.
- (22) Massiot, Ph.; Centeno, M. A.; Carrizosa, I.; Odriozola, J. A. *J. Non-Cryst. Solids* **2001**, *292*, 158–166.
- (23) (a) Gao, W.; Dickinson, L.; Grozinger, C.; Morin, F. G.; Reven, L. *Langmuir* **1996**, *12*, 6429–6435. (b) Frost, R. L.; Kristof, J. *Clays Clay Miner.* **1997**, *45*, 551–563. (c) Madejova, J.; Komadel, P. *Clays Clay Miner.* **2001**, *49*, 410–432.
- (24) (a) Earl, W. L.; VanderHart, D. L. *Macromolecules* **1979**, *12*, 762–767. (b) Tonelli, A. E.; Schilling, F. C. *Acc. Chem. Res.* **1981**, *14*, 233–238.
- (25) Pursch, M.; Strohschein, S.; Händel, H.; Albert, K. *Anal. Chem.* **1996**, *68*, 386–393.
- (26) (a) Cao, G.; Hong, H. -G.; Mallouk, T. E. *Acc. Chem. Res.* **1992**, *25*, 420–427. (b) Lynch, V. M.; Mallouk, T. E. *Inorg. Chem.* **1988**, *27*, 2781–2785.
- (27) (a) McNatt, J. S.; Morgan, J. M.; Farkas, N.; Ramsier, R. D. *Langmuir* **2003**, *19*, 1148–1153. (b) Holland, G. P.; Sharma, R.; Agola, J. O.; Amin, S.; Solomon, V. C.; Singh, P.; Buttry, D. A.; Yarger, J. L. *Chem. Mater.* **2007**, *19*, 2519–2526. (c) Lurkes, I.; Borbaruah, M.; Quin, L. D. *J. Am. Chem. Soc.* **1994**, *116*, 1737–1741. (d) Sasaki, D. Y.; Alam, T. M. *Chem. Mater.* **2000**, *12*, 1400–1407. (e) Pawsey, S.; McCormick, M.; De Paul, S.; Graf, R.; Lee, Y. S.; Reven, L.; Spiess, H. W. *J. Am. Chem. Soc.* **2003**, *125*, 4174–4184.
- (28) Corriu, R. J. P.; Leclercq, D.; Mutin, P. H.; Sarlin, L.; Vioux, A. *J. Mater. Chem.* **1998**, *8*, 1827–1833.
- (29) Ellis, R. L.; Nelson, R. D. *Spectrochim. Acta* **1958**, *10*, 307–329.
- (30) (a) Higuchi, T. *J. Pharm. Sci.* **1961**, *50*, 874–875. (b) Higuchi, T. *J. Pharm. Sci.* **1963**, *52*, 1145–1149.
- (31) (a) Vallet-Regí, M.; Balas, F.; Acros, D. *Angew. Chem., Int. Ed.* **2007**, *46*, 7548–7558. (b) Munoz, B.; Rámila, A.; Pérez-Pariente, J.; Díaz, I.; Vallet-Regí, M. *Chem. Mater.* **2003**, *15*, 500–503. (c) Anderson, J.; Rosenholm, J.; Areva, S.; Linden, M. *Chem. Mater.* **2004**, *16*, 4160–4164.